



Source Spectra of Near Kamchatka Earthquakes: Recovering them from *S*-Wave Spectra, and Determination of Scaling for Three Corner Frequencies

A. A. GUSEV^{1,2} and E. M. GUSEVA²

Abstract—We describe a procedure for mass determination of the “source-controlled f_{\max} ”—an important though not conventional parameter of earthquake source spectrum, relabeled here as “the third corner frequency,” f_{c3} , and discuss the results of its application. f_{\max} is the upper cutoff frequency of Fourier acceleration spectrum of a record of a local earthquake; both source and path attenuation contribute to f_{\max} . Most researchers believe the role of attenuation (“ κ ” parameter) to be dominating or exclusive. Still, source effect on f_{\max} is sometimes revealed. If real, it may be important for source physics. To understand better the f_{\max} phenomena, the constituents of f_{\max} must be accurately separated. With this goal, we process seismograms of moderate earthquakes from Kamchatka subduction zone. First, we need reliable estimates of attenuation to recover source spectra. To this goal, an iterative processing procedure is constructed, that adjusts the attenuation model until the recovered source acceleration spectra become, on the average, flat up either to f_{c3} , or up to the high-frequency limit of the frequency range analyzed. The latter case occurs when f_{c3} is non-existent or unobservable. Below f_{c3} , the double-corner source spectral model is thought to be valid, and the lower bound of acceleration spectral plateau is considered as the second corner frequency of earthquake source spectrum, f_{c2} . The common corner frequency, f_{c1} , is also estimated. Following this approach, more than 500 *S*-wave spectra of $M = 4$ –6.5 Kamchatka earthquakes with hypocentral distances 80–220 km were analyzed. In about 80 % of the cases, f_{c3} is clearly manifested; the remaining cases show, at high frequency, flat source acceleration spectra. In addition, in about 2/3 of cases, f_{c2} is clearly above f_{c1} , showing that double-corner spectra may dominate even at moderate magnitudes. Scaling behavior was examined for each of the corners. The f_{c1} vs. M_0 trend is common and close to similarity ($f_{c1} \propto M_0^{-1/3}$), whereas the trends for two other corners ($f_{c2} \propto M_0^{-0.17}$; $f_{c3} \propto M_0^{-0.11}$) dramatically contradict the concept of similarity. Physical interpretation of such a behavior is discussed. The origin of f_{c3} is ascribed to existence of the lowermost wavelength/size of fault heterogeneity. Its dependence on M_0 may reflect evolution of maturity of a fault in geological time. The approximate scaling $f_{c2} \propto f_{c1}^{0.5}$ suggests that during propagation of slip pulse over a fault, its width, assumedly related to $1/f_{c2}$, grows in a stochastic manner; this

reminds the random evolution of propagating boundary in the framework of the known Eden model of random growth.

Key words: Earthquake fault, spectrum, scaling, f_{\max} , κ , path, attenuation.

1. Introduction

The classical models of earthquake source spectrum after AKI (1967) and BRUNE (1970) have ω^{-2} high-frequency (HF) asymptote and thus flat acceleration spectrum $a(f)$. HANKS (1982) paid attention to the “ f_{\max} ” phenomenon: $a(f)$ of a record shows HF cutoff, and it does not disappear after correction for path-related loss. GUSEV (1983) and PAPAGEORGIU and AKI (1983) ascribed the origin of this cutoff to the source; later AKI (1988) noticed that f_{\max} slowly decreases with magnitude, and treated this fact as supporting this idea. However, ANDERSON and HOUGH (1984) have shown convincingly that a near-site constant- Q attenuation layer of limited thickness commonly exists, that introduces distance-independent loss; this factor can explain the f_{\max} feature without any source-related effects. The idea of source origin of f_{\max} lost support and was, essentially, abandoned. Still, evidence has been accumulated step by step suggesting that the formation of f_{\max} is a complex phenomenon that incorporates both site-controlled and source-controlled constituents, see the study by GUSEV (2013a) for a review. This source-controlled constituent f_{\max} will be the main object of the present study, and will be denoted f_{c3} , the third corner frequency. This denotation hints that below f_{c3} , two corners are typically present, that jointly provide the bend of displacement spectrum from f^0 to

¹ Institute of Seismology and Volcanology, Far East Division, Russian Ac. Sci., Piip Blvd. 9, Petropavlovsk-Kamchatsky 683006, Russia. E-mail: gusev@emsd.ru

² Kamchatka Branch, Geophysical Survey, Russian Ac. Sci., Piip Blvd. 9, Petropavlovsk-Kamchatsky 683006, Russia.

f^{-2} behavior, as was proposed by BRUNE (1970) and supported by data analysis after GUSEV (1983); positions of these corners will be denoted as f_{c1} and f_{c2} .

ANDERSON and HOUGH (1984) introduced κ parameter to describe loss-related low-pass filter; its cutoff frequency will be denoted f_κ . This filter modifies source-generated signal; this complicates detection and (if found) estimation of f_{c3} . Figure 1 sketches out how site and source factors interfere; it makes clear why it is a difficult task to determine separately both f_{c3} and f_κ . Note that the problem was well understood by ANDERSON and HOUGH (1984); see their Fig. 13. ATKINSON (1996) found some indications to combined effect of these factors. To obtain more decisive results regarding the existence of f_{c3} , i.e., to suppress the effects of f_κ , two techniques were tried: to use instruments located in a deep borehole (KINOSHITA 1992; SATOH *et al.* 1997); or to use ratios of spectra of two earthquakes with widely different f_{c3} , recorded by the same station. In the last case, the effects of “ f_κ -filter” and also of site amplification filter cancel out (YOKOI and IRIKURA 1991; SASATANI 1997); path contributions may be different but this

difference is known better and can be compensated for. See the study by GUSEV (2013a) for more examples and a short review. The spectral ratio approach may produce illuminating examples (POPESCU *et al.* 2003), but it is not appropriate for establishing general tendencies.

Both the existence and behavior of f_{c3} represent interesting research topics; their study may provide important information about the structure of earthquake source and dynamic processes within it. It is now a common idea that the HF part of source spectrum is formed by multiple-scaled heterogeneity, seemingly of the fractal kind. It can represent random field of stress drop, of random strength, or of random relief of fault wall. The f_{c3} parameter, if real, is a manifestation of the lower fractal limit of heterogeneity size/wavelength; i.e., it is an imprint of the upper cutoff of its wavenumber spectrum (PAPAGEORGIOU and AKI 1983; AKI 1988).

In engineering seismology, there is a need for accurate and stable estimates of the loss parameter, κ . When the effects of f_{c3} are present but ignored, a certain part of the observed HF spectral decay that is

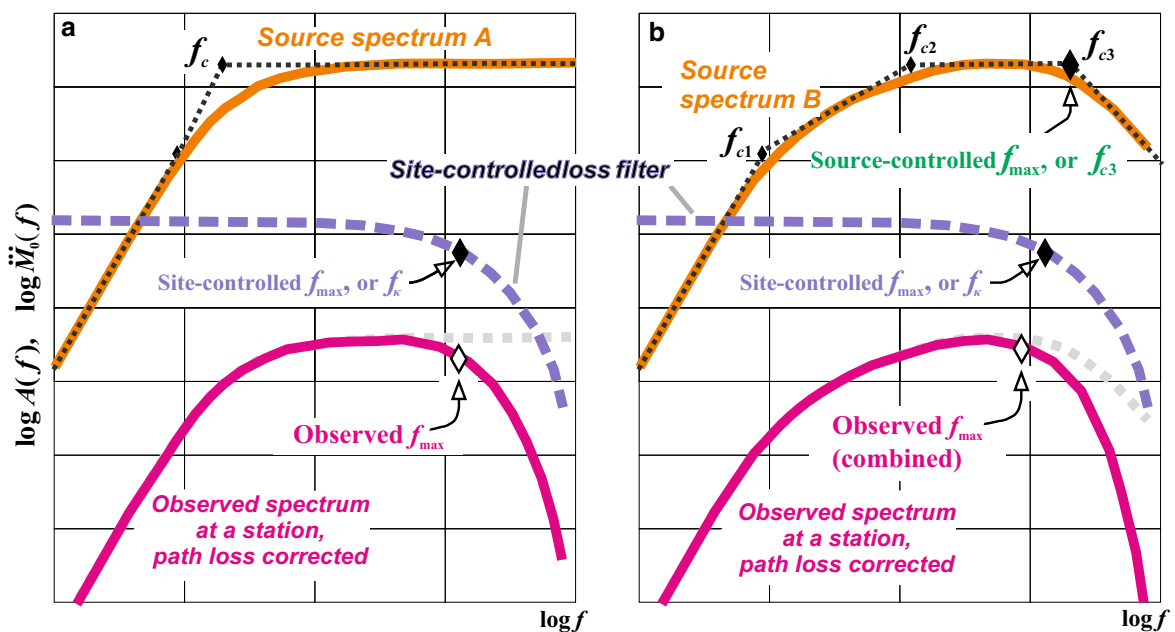


Figure 1

A sketch of Fourier acceleration spectrum of body waves, for two versions of source acceleration spectrum ($\ddot{M}_0(f)$ or SAS): single-corner one (a), and three-corner one (b). Top curves (orange in color version) are SAS, bottom curves (magenta in color version) are acceleration spectra $A(f)$ at a station, corrected for path-related loss. The middle curve (blue in color version) is a typical transfer function of the attenuating near-site layer. See text for more details

of source origin is treated as a site effect; this may perturb and even systematically bias κ_0 estimates, as explained later. KILB *et al.* (2012) note that “the scatter within kappa measurements at a given station is likely caused by a significant contribution from near the source”; they, however, relate this contribution not to the source spectrum, but rather, to near-source scatterers. Generally, the knowledge of f_{c3} is significant for accurate prediction of peak accelerations, especially at near-fault sites, as it directly affects the upper spectral cutoff. Therefore, a method for systematic separation of source and path contributions to f_{\max} is of clear practical importance.

The analysis of the decay of acceleration spectra at HF, parameterized by κ , was done by Purvance and ANDERSON (2003) for a large data set from Mexico. Empirical κ estimates were processed by least squares to split them into separate contributions from source (κ_{event}) and site (κ_{site} , hereinafter denoted κ_0). High statistical significance of source contribution was accurately proven; but the geophysical results were limited, possibly because the frequency dependence of loss was ignored. Attention to this factor is an important point of the present study. An important result of the recent studies of κ is the understanding of significant uncertainty of station κ_0 estimates obtained by various methods (EDWARDS *et al.* 2015; KILB *et al.* 2012). Source contribution to this uncertainty may be significant sometimes.

An interesting field of study is that of scaling behavior of fault parameters, and in particular of corner frequencies: f_{c1} , f_{c2} , and f_{c3} . These parameters will be shortly denoted as f_{ci} . When discussing scaling of f_{ci} , one can take as a reference the concept of similarity of earthquake source geometry and kinematics. As shown by KANAMORI and ANDERSON (1975), the similarity concept is approximately valid for large earthquakes. For small-to-moderate ones its applicability, often formulated as a question of magnitude dependence of stress drop, is a matter of active discussion (see e.g., BALTAY *et al.* 2011). As an independent variable in similarity studies, the seismic moment M_0 is commonly taken, and the scaling relationships for f_{ci} are written in the form $f_{ci} \propto M_0^{-\beta_i}$. The common topic is the scaling of f_{c1} (related to inverse rupture duration) which, in case of similarity, follows $f_{c1} \propto M_0^{-1/3}$, so that $\beta_1 = 1/3$. Our data on f_{c1}

do not indicate violation of similarity, as will be seen. Less elaborated is the question of scaling of f_{c2} and f_{c3} trend. What can be assumed a priori is that in case of similarity, scaling of each of f_{ci} must be identical, as these parameters have the same dimension, so that all β_i can be expected to be equal to 1/3, and the shape of source spectrum is identical, in the log–log scale, at any M_0 . Deviations of real source spectra from similarity bear information on the properties of fault rupture. GUSEV (2013a) reviewed published trends of f_{c2} and f_{c3} and found $\beta_2 = 0.17$ and $\beta_3 = 0.08$ as typical values; thus, similarity appears to be violated with respect both to f_{c2} and f_{c3} . Most of these results are preliminary, and further studies are evidently needed.

During 1993–2005, a single Kamchatka broadband (BB) station PET produced a considerable amount of records that permitted to study f_{\max} phenomena. At the exploration stage of this work, GUSEV and GUSEVA (2014) apparently revealed the existence of f_{c3} for a significant fraction of cases. In that letter, however, to recover source spectra from S -wave spectra, a preliminary attenuation model was used. For this reason, the obtained interesting results could not be considered as firmly established. For a mass study of f_{c3} to be convincing, a more reliable attenuation model should be used instead. This goal was achieved in two steps. The first step was to design a novel method of spectrum-based inversion for attenuation (GUSEV and GUSEVA 2016). Its idea is to use, in inversion for attenuation model, only the parts of observed spectra that are below f_{c3} . The already determined set of f_{c3} was used, and an adjusted attenuation model was obtained, with only limited difference from the trial one. But it was not possible to be satisfied by this fact. In principle, any change in attenuation model must entail revision of all f_{c3} estimates. One cannot be sure beforehand that iterations of the two-phase procedure—(1) adjust attenuation model, then (2) revise f_{c3} estimates—will converge. In the present study, just this iterative adjustment of both attenuation model and f_{c3} set is performed. As an interesting side results of this research, sets of f_{c1} and f_{c2} values were also determined.

The plan of the study is as follows. First, a reliable attenuation model is found following the above-described iterative scheme. On convergence of the

iterative loop, the obtained set of spectral corners is analyzed in terms of scaling behavior. Finally, the recovered scaling trends are discussed, and some hypotheses are proposed regarding their possible physical meaning.

2. The Complex Nature of Acceleration Spectral Cutoff and the General Approach of the Study

As an introductory step let us consider how source spectrum shape is modified during wave propagation in a medium with energy loss. Earthquake source time history can be described by seismic moment rate $\dot{M}_0(t)$, i.e., source time function, with its amplitude spectrum $\dot{M}_0(f)$, or source spectrum. Source acceleration spectrum (SAS), $\ddot{M}_0(f)$, equals $(2\pi)^2 \dot{M}_0(f)$. In Fig. 1, two idealized versions of SAS are depicted. One version (a) has a single corner at the lower frequency (LF) side, located at f_c ; another (b) has a double (split) corner here, whose components are located at f_{c1} and f_{c2} . Both models follow BRUNE (1970); both are of the “ ω^{-2} ” kind; this “ ω^{-2} ” part of source spectrum is transformed into a corresponding “plateau” in SAS. At the HF side, the SAS “b” has a cutoff at f_{c3} ; then it decays as $f^{-\varepsilon}$, with estimated ε on the order 1–2 (i.e., the exponent is 3–4 for source spectrum). The SAS “a” is flat at HF ($f_{c3} \rightarrow \infty$). The more general three-cornered SAS “b” is considered realistic in this paper; it transforms into “a” by setting $f_c = f_{c1} = f_{c2}$, and $f_{c3} \rightarrow \infty$. At the bottom of the plot, corresponding observed acceleration spectra $A(f)$ at a station are given, after along-path loss correction; i.e., only the loss related to the medium layer immediately under the station takes effect. The middle shape is a typical transfer function of this attenuating near-site layer, which contributes to formation of the upper cutoff of the spectrum of a record. Another contribution is distance related and not considered here. This filter is parameterized by its upper cutoff frequency, f_κ , or site-controlled [constituent of f_{\max}]. Generally, f_{\max} may be associated with total (path plus site) effect parameterized by κ , expressing, therefore, the property of the spectrum of a record; or solely with site-only effect, parameterized by κ_0 . If the second definition is considered as preferable, as we do, the spectrum of a record must be path-corrected before picking f_{\max} . HANKS (1982) is not fully

strict in associating f_{\max} solely with site effect. There are no ready denotations for these two variants of f_{\max} definition, and this may create some confusion. In the discussion of Fig. 1, f_{\max} is associated specifically with κ_0 ; in the case of flat acceleration spectrum, it equals f_κ . To relate f_κ to κ_0 one can use either -3 dB (50 % power) cutoff that results in $f_\kappa = \log_e(2)/2\pi\kappa_0 \approx 0.11/\kappa_0$ or -6 dB (50 % amplitude) cutoff, resulting in $f_\kappa \approx 0.22/\kappa_0$; other definitions are possible. The assumed (b) kind of SAS has three corner frequencies f_{c1} , f_{c2} and f_{c3} ; the latter is a new short denotation for the “source-controlled [constituent of] f_{\max} ”. The two cutoffs, at f_κ and at f_{c3} , operating jointly, produce a combined or “summary” cutoff at an “observed f_{\max} ”, with its value below that of each of its constituents. The distance-related loss, ignored in this argument, would result in even lower observed f_{\max} . An important fact can be seen from Fig. 1: when f_{c3} is actually finite, but during the data analysis one assumes that $f_{c3} \rightarrow \infty$, a negative bias in the f_κ estimate will appear; correspondingly, κ_0 will be overestimated.

Let us consider the loss operator that affects a record in more detail. ANDERSON and HOUGH (1984) realized that propagation loss, expressed by the κ parameter, can be split into a distance-independent, site-related component, κ_0 , and a distance-dependent one, $\tilde{\kappa}$ [denoted following ANDERSON (1991)]. The middle curve in Fig. 1 is related to κ_0 . To estimate true source spectrum from the observed body-wave spectrum, i.e., to compensate loss, one needs its parameters, both κ_0 , and $\tilde{\kappa}$. Unfortunately, neither direct inversion of station network data nor the use of less noisy coda-normalized data cannot recover a complete attenuation picture. Only $\tilde{\kappa}$ can be recovered, whereas κ_0 is rarely observable in this manner. To find κ_0 , one might, and often do, use the spectral method, making, however, an assumption that SAS is flat at HF. This assumption is difficult to verify; real spectra may and sometimes do violate it, as described in Introduction. An attempt to overcome this difficulty is the main point of the present study: the list of unknowns to be sought for will include κ_0 , frequency-dependent $\tilde{\kappa}$ and finite f_{c3} values; the latter provide the upper bound of the part of the spectrum usable in the inversion for $Q(f)$.

The determination of these unknowns is carried out in two steps. As a first step, a realistic preliminary

loss model is used for spectral correction. Then, either f_{c3} values are estimated from the recovered spectra, or the absence of any observable upper cutoff of SAS is recorded. Denote the upper cutoff of observable flat SAS as f_H ; it can be equal to f_{c3} , or merely describe the uppermost resolvable frequency. This upper limit can be produced either by too low S/N ratio or by the proximity of the Nyquist frequency of digitized data. At the LF side, the lowermost usable frequency is defined either by f_{c2} , (or sometimes by $f_{c1} = f_{c2}$), or by surface-wave contamination, or again by low S/N values, now at the LF edge. Denote this LF bound of the work range as f_L . The limited segments of observed spectra, between f_L and f_H , can be used then in the traditional way to recover an adjusted attenuation model by the spectral method.

3. Data and Their Processing

3.1. Data

The collected data set consists of records of station PET including those of the low-gain HN channel of IRIS BB station (with FBA-23 accelerometer), digitized at 80 sps, for 1993–2005 (433 records); and of the Guralp CMG5T accelerometer, with sampling frequency 100 sps, for 2006–2008 (130 records). We use records of local earthquakes at hypocentral distances $r = 80$ –220 km. The depth range is 0–200 km, mostly 0–50 km, $M_L = 4$ –6.5 ($M_L \approx M_w + 0.35$, as further explained). Source epicenters are shown in Fig. 2. This data set was used for such tasks as: qualitative examination of observed and source-reduced (i.e., loss-corrected) spectra; estimation of f_{c1} , f_{c2} and f_{c3} , or, shortly, f_{ci} , and iterative adjustment of the attenuation model. In all cases, the frequency range up to $0.75 f_{Nyquist}$ (i.e., up to 30 or 37 Hz) was considered.

3.2. Possible Site Effect on Spectra

A possible obstacle for the spectral method is the effect of site geology (site response). Specifically for PET station, these effects were never noticed in tens of microzoning studies when PET was the reference

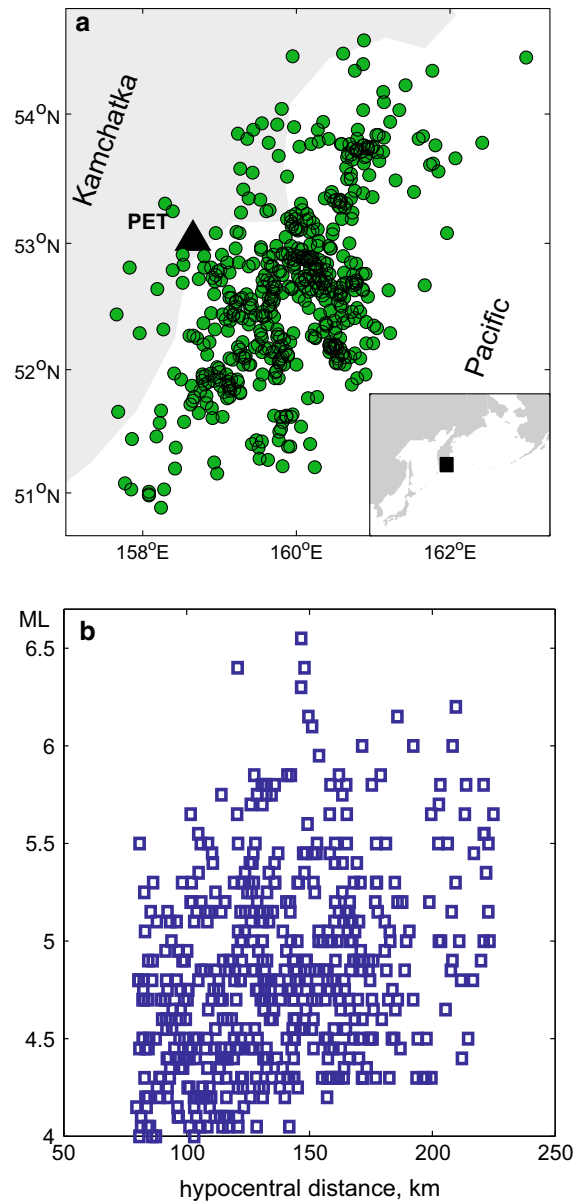


Figure 2
Distribution of 563 earthquakes used. **a** Epicenters and location of seismic station PET. **b** Data distribution over hypocentral distance and magnitude

hard-rock station (if such effects were significant, they would be seen at least sometimes as holes or negative trends in spectral ratios). In another two detailed studies of spectral properties of PET based on the HVR method (horizontal to vertical spectral ratios), one that employed direct S-waves, and

another with coda waves, again no indication of site anomalies were found over the 1–25 Hz range. There exist some studies of the vertical structure of upper crustal layering under PET. From these data, it was found in (GUSEV and GUSEVA 2016) that the lower impedance layering of the upper 500 m of the profile can amplify high frequencies and, therefore, distort the estimate of κ_0 shifting it to lower values. Such a distortion may be significant. For instance, among 15 hard-rock stations in South Korea studied by JO and BAAG (2007), seven showed zero or negative κ_0 estimates. To find possible distortion, the quarter-wavelength approximation was used following Boore and Joyner (1997); the estimated spectral amplification was converted to possible κ_0 adjustment. Its value was estimated as 0.006–0.007 s, comparable to the accuracy of our estimates of κ_0 , and was not taken into account.

3.3. Determination of Smoothed Spectra

On a digital trace, the *S*-wave group was selected interactively, with visually picked window duration of 10–35 % of *S*-wave travel time. The wide range of used durations is related to their evident wide variation related probably to differences in along-ray scattering. In particular, lower depth events typically produce longer *S*-wave groups because of expressed depth dependence of scattering, as discussed by ABUBAKIROV and GUSEV (1990). Alternatively, automatically selected duration of 25 % of *S*-wave travel time was tried, with hardly noticeable change of results. The former, interactive, procedure was finally used. The segment of instrument-corrected acceleration signal was cut out, tapered at 0–5 and 95–100 % of the full duration, and processed by FFT. The resulting discrete spectrum was smoothed using spectral window of log-uniform width of 0.5 octave (at –3 dB level) or 0.15 decade in $\log_{10}(f)$ units. The step along the *f*-axis is also log-uniform and equals 0.05 (20 points per decade). A noise window of comparable or longer duration, selected before the *P* onset, was processed in the same manner; its spectral energy was adjusted for the difference of durations of the windows, and represented background noise. For *S*-wave spectra in the mentioned time window, the rms amplitude of a

single component was determined over two horizontal components.

3.4. Initial Loss Model

To obtain approximate estimates of source spectra, an initial loss model was needed to calculate the first variant of loss corrections. At the first stage of entire study it was compiled on the basis of the earlier work on *S*-wave attenuation in this area. The main sources used are as follows (Fig. 3). For the 1–6 Hz band, ABUBAKIROV (2005) estimated $Q_S(f)$ using distance decay of coda-normalized spectral levels of band-filtered data; *S*-wave spectra were calculated over the 5-s data window. For the 5–25 Hz band the results of GUSEV and GUSEVA (2012) were used. They determined *S*-wave κ values only from spectra that covered the entire 5–25 Hz band; therefore, they implicitly excluded a large fraction of events with low f_{c3} that might bias (artificially increase) loss estimates, as already explained. No frequency dependence of related quality factor $Q_S = Q$ was assumed in that study and, therefore, three variants of possible

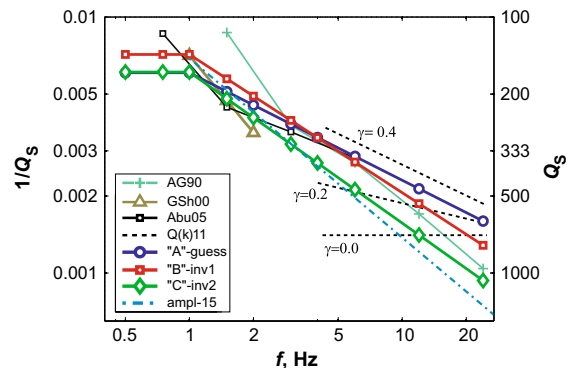


Figure 3

Variants of frequency dependence of Q^{-1} at the distance $r = 100$ km near PET. The curve labels denote: *AG90*: (ABUBAKIROV and GUSEV 1990), coda and direct waves interpreted using numerical simulation of multiple scattering; *GSh99*: (GUSEV and SHUMILINA 2000), interpretation of the decay of macroseismic intensity, frequency binding uncertain; *Abu05*: (ABUBAKIROV 2005), inversion of the distance decay of spectral amplitude; *Q(k)11*: variants of $Q^{-1}(f)$ converted from κ estimates of GUSEV and GUSEVA (2012), see text for details; *"A"-guess*: initial approximation based on compilation of earlier research (GUSEV and GUSEVA 2014); *"B"-inv1*, *"C"-inv2*: results of two successive inversions, see text and Table 1; *ampl-15*: a preliminary estimate from the spectral amplitude decay with distance

Table 1

Attenuation models for Kamchatka subduction zone, and recovered parameters of scaling

Model	Attenuation parameters				Parameters of scaling*			Reference and comment
	κ_0 , s	Q_0	γ	q	β_1	β_2	β_3	
“A”	0.016	165	0.42	-0.36	0.32	0.17	0.08	(GUSEV and GUSEVA 2014). Model “A” is compiled and the f_{c3} set “A” is determined
“B”	0.027 ± 0.007	140 ± 35	0.54 ± 0.08	-0.18 ± 0.08	n/a	n/a	0.08	(GUSEV and GUSEVA 2016). The f_{c3} set “A” is used in inversion, which resulted in model “B”
“C”	0.034	164	0.59	-0.17	0.33	0.17	0.11	Current paper. Using model “B”, the f_{c3} set “B” is determined; it is then used in inversion which resulted in model “C”
“CP”	0.015	150	0.43	n/a	n/a	n/a	n/a	Current paper. Modification of model “C”

Formal standard errors for β_i are all below 0.03. For β_1 , the orthogonal regression estimates are given

* $\beta_i = d \log f_{ci} / d \log M_0$

$Q(f)$ lines are plotted in Fig. 3 that fit the estimated κ value over the 5–25 Hz frequency range assuming $\tilde{\kappa}$ and Q^{-1} proportional to f^0 , $f^{-0.2}$ and $f^{-0.4}$. Some other estimates were also taken into account, see Fig. 3. The final accepted trend for $r = 100$ km is $Q_S(f) = 165 f^{0.42}$. In addition, the value $\kappa_0 = 0.016$ s was accepted.

GUSEV and GUSEVA (2012) found that near PET, the dependence of κ on hypocentral distance r is clearly convex, indicating diminution of loss with distance. From these data, a rough estimate of the distance dependence of loss was constructed in a simplest form, with linear decay of Q^{-1} . The final loss representation is:

$$\begin{aligned} -\log_e \left(\frac{A(f)}{A_0(f)} \right) &= \pi f (\kappa_0 + \tilde{\kappa}) \\ &= \pi f \kappa_0 + \left(\frac{r}{c} \right) Q^{-1}(f, r) = \pi f \kappa(f, r) \end{aligned} \quad (1)$$

where $A(f)$ and $A_0(f)$ are spectral amplitudes for the cases when loss is present or absent, correspondingly, $c = 3.8$ km/s is S -wave velocity; and $Q(f, r)$ is distance-dependent path quality factor:

$$Q^{-1}(f, r) = Q_0^{-1} \left(\frac{f}{f_0} \right)^{-\gamma} \left(1 + q \frac{r - r_0}{r_0} \right) \quad (2)$$

with the reference distance r_0 set at 100 km, reference frequency f_0 set at 1 Hz, and the negative

q parameter describes how attenuation diminishes with distance. Below f_0 , $Q^{-1}(f) = Q^{-1}(f_0)$. The entire initial attenuation model is called “A” hereinafter (Table 1).

3.5. Interactive processing of spectra

The calculated S -wave spectra were represented as those of displacement $d_0(f)$, velocity $v_0(f)$ and acceleration $a_0(f)$; see example in Fig. 4. In addition, the loss-corrected versions of these spectra were calculated, denoted hereinafter, respectfully, as $d(f)$, $v(f)$ and $a(f)$. Noise spectra are also shown. On a $d(f)$ plot, the f_{c1} corner position (abscissa: f_{c1} , ordinate: LF spectral level) was selected. Similarly, on a $v(f)$ plot, f_{c1} corner (second estimate) and f_{c2} corner were selected. On $a(f)$ plot, f_{c2} corner (second estimate) and f_{c3} corner were picked. Figure 4 shows the case when all these corners are well expressed and discernible. In the practical work, some of the corners could not be picked reliably. In a considerable fraction of cases, f_{c3} was not discernible, see Fig. 5. This situation, that agrees with the ω^{-2} spectral asymptote, could arise in two cases: the spectrum as such is above noise up to the highest considered point, (30 or 37 Hz), or the uppermost observable point is below this bound because of the high S/N ratio. In a limited number of cases, no confident judgment regarding f_{c3} was possible

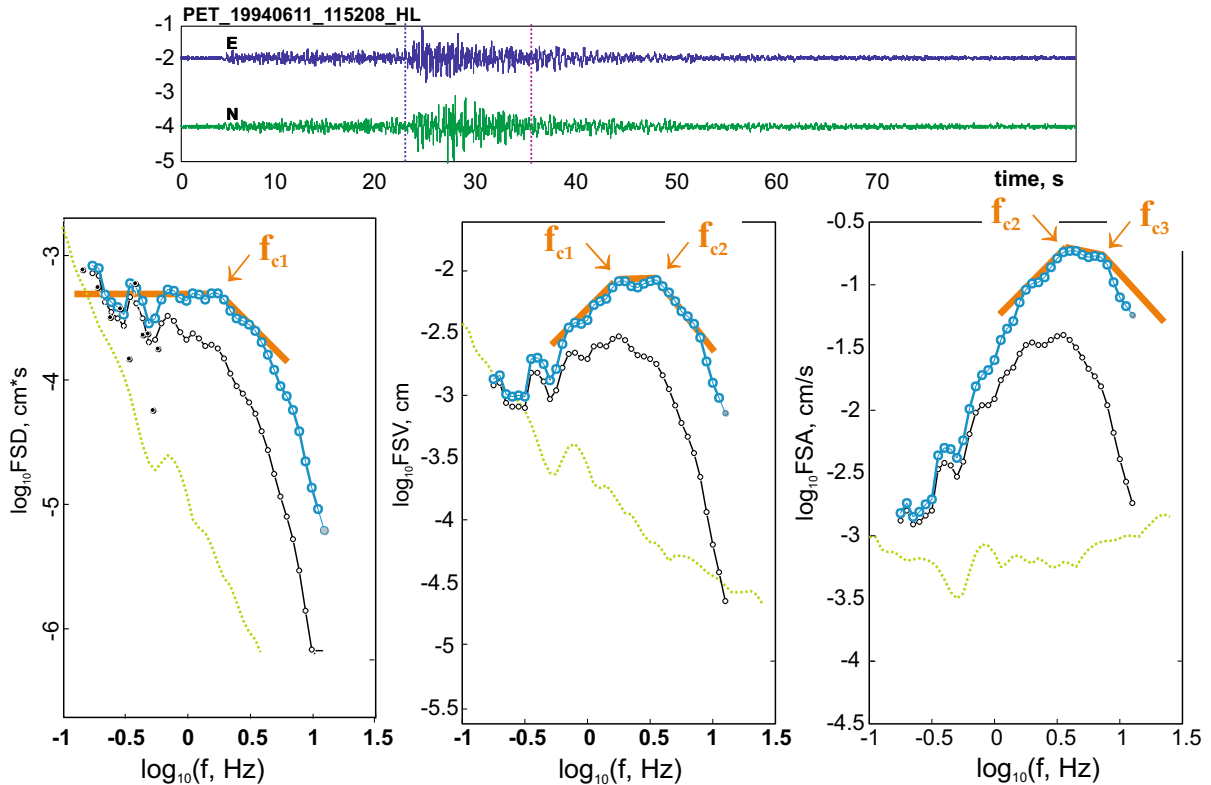


Figure 4

An example of picking corner frequencies f_{c1} , f_{c2} and f_{c3} in the interactive mode. *Top box* shows horizontal acceleration traces with selected S -wave window shown by *dotted lines*; *three lower boxes* show, *left to right*, smoothed $d(f)$, $v(f)$ and $a(f)$ spectra. In each of these *boxes*, *upper* (blue in color plot) curve is the attenuation-corrected spectrum, *black curve* under it is the observed spectrum, and *dashes* below show noise level. *Knees on thick segmented lines* (orange in color plot) show the actual interactive selection of spectral corners: f_{c1} on the $d(f)$ plot; f_{c1} (another pick) and f_{c2} on the $v(f)$ plot; f_{c2} (another pick) and f_{c3} on the $a(f)$ plot

because of a complicated spectral shape. At any rate, the upper bound of the workable $a(f)$ spectrum, or f_H , was determined. As for the similar lower bound, f_L , it almost always coincided with f_{c2} . The “plateau” between f_L and f_H was permitted not to be accurately flat, because it is impossible, through applying a single set of attenuation parameters, to make all recovered spectra perfectly flat.

At the LF side, the expected spectral plateau on the $d(f)$ spectrum was sometimes uncertain or not seen at all, preventing the determination of f_{c1} and of $d(f | f \rightarrow 0)$. This is due to low S/N ratio for lower magnitudes, and/or to the probable contamination of spectrum by surface waves for larger magnitudes; in all, no reliable f_{c1} estimate was possible for 15 % of spectra. When selecting f_{c3} , it

was required that above f_{c3} , the decay of corrected spectrum: (1) is sufficiently steep, i.e., with log–log slope above 0.5; and (2) is supported by at least three points of the smoothed spectrum (i.e., over the f range of at least 0.15 decade). As a rule, the log–log slopes of $a(f)$ below f_{c3} were in the range $-(0.8-1.6)$. Cases of combined corners, with $f_{c1} \approx f_{c2}$, or $f_{c2} \approx f_{c3}$, were common. As the final estimate of f_{c1} , the geometric average of the two picks made on $d(f)$ and $v(f)$ windows was used; similar procedure was performed for f_{c2} , using picks from $v(f)$ and $a(f)$ windows.

“Sharp” shapes of corners are well seen in Figs. 4 and 5. This feature of real spectra is common for our spectral plots despite considerable smoothing that could suppress it. Most corners of our spectral shapes

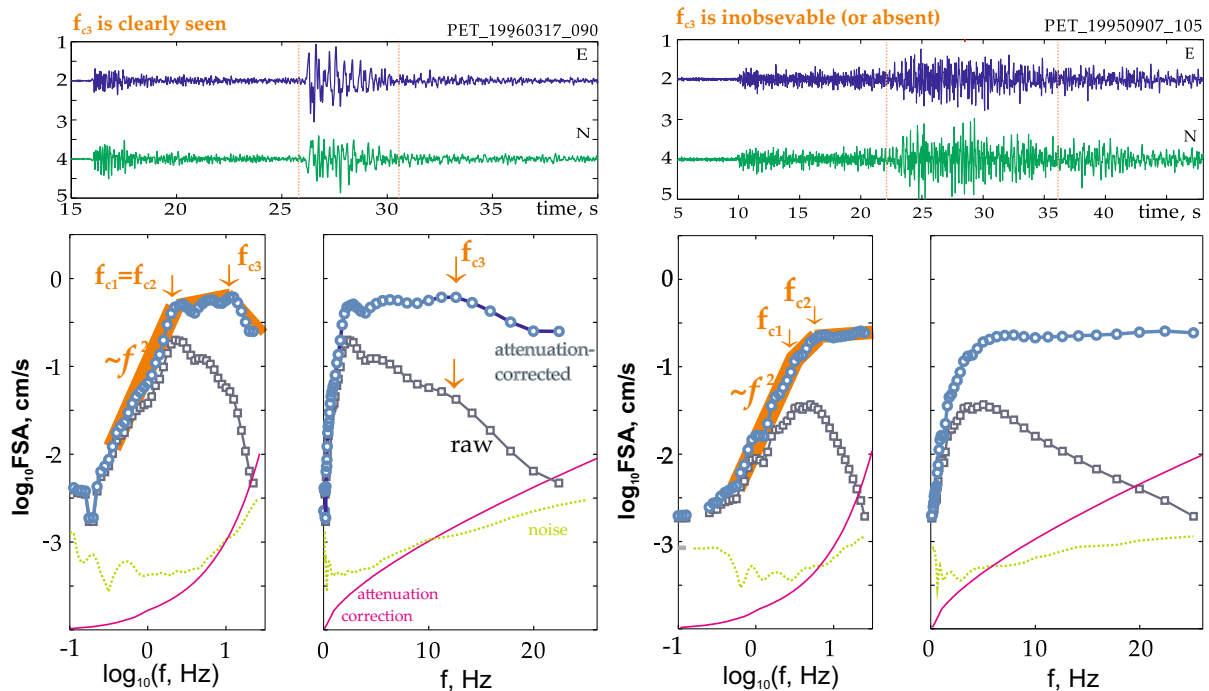


Figure 5

Two examples of picking corner frequencies f_{c2} and f_{c3} in interactive mode, for two events. Each event is represented by a group of *three plot boxes*: horizontal traces on top and $a(f)$ spectra in log–log (left bottom box) and log–linear (right bottom box) scales. Curves are similar to $a(f)$ curves of Fig. 4, with addition of a thin line (red in color version) that represents attenuation correction. The left group is for the case with well-discernible f_{c3} , whereas the right group is for the case with no f_{c3} seen up to 30 Hz

are clearly less blunt than predicted by BRUNE'S (1970) single-corner as well as AKI'S (1967) or JOYNER'S (1984) double-corner spectral models; typically they are comparable to or even sharper than the $(1 + (f/f_c)^4)^{-1/2}$ shape proposed in (BOATWRIGHT 1978).

In Fig. 5, we present the cases of observable and unobservable (or absent) f_{c3} corner. In addition, this picture illustrates why f_{c3} is difficult to notice when working in the log–linear scale traditional in determination of κ . As clearly seen from the left plot in Fig. 5a, the f_{c3} corner is evident on the loss-corrected plot in the log–log scale; whereas on the uncorrected plot in the log–linear scale, the presence of the same corner is near to unnoticeable even on the smoothed spectrum (On the original unsmoothed spectrum, the chances to identify this corner will be even less). This situation may be typical, potentially leading to a broad scatter of κ estimates. The scatter of this kind was found in particular for the PET data when studied

in a simpler way in (GUSEV and GUSEVA 2012), using plots in the log–linear scale.

In the described way, f_{c2} or f_L , and f_{c3} or f_H , frequencies, and also f_{c1} , were determined for a considerable part of 433 spectra studied at the first stage of work. The typical range of f_L , and of f_H , can be seen from the distribution of f_{c3} , f_{c2} values depicted on the scattergrams in Fig. 8b, c below. The obtained trends of f_{ci} , with respect to local magnitude, have been published in the short paper (GUSEV and GUSEVA 2014). The results were intriguing. First, f_{c3} was reliably identified in majority of cases. Second, clear indications of non-similarity of scaling were found for f_{c2} and the more so for f_{c3} , whereas the data for f_{c1} did not contradict the similarity concept. These preliminary results needed an accurate checkup. In particular, the attenuation model used for spectral correction had to be refined and verified. This is done in the following.

4. Improving the S-Wave Attenuation Model

It was expedient to determine a new adjusted attenuation model, to prevent systematic errors in estimation of f_{c3} caused by a possible bias in the assumed loss; and the accumulated data were used to make inversion for such model. The functional description of attenuation transfer function as expressed by Eqs. 1 and 2 was used again; the same $r_0 = 100$ km and $c = 3.8$ km/s were also used. The set of unknown parameters is $\{Q_0^{-1}, \gamma, q, \kappa_0\}$, or compactly $x_k = \{x_1, x_2, x_3, x_4\}$; see Table 1 for x_k of the initial (or “A”) and successive models. The

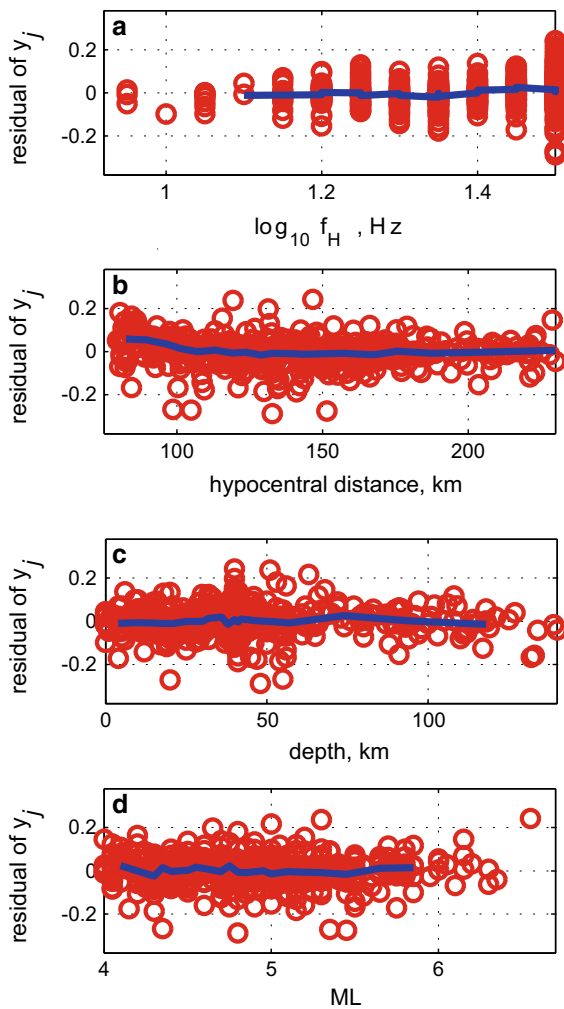


Figure 6

Residuals of fitting y_j by the “C” attenuation model plotted against f_H (a), r (b), depth (c) and M_L (d) as circles (red), and their running median as continuous line (blue)

observational data used in inversion consisted of spectral amplitudes A_L and A_H , picked from uncorrected spectra at the frequencies f_L and f_H . Introduce observables $y_j = \log_e A_H/A_L$, where $j = 1, 2, \dots, N$ enumerates the observed spectra. From (1) and (2), the theoretical value for y_j is

$$\begin{aligned} y_{j,theo} &= F_j(x_k) \\ &= -\pi Q_0^{-1} (f_H^{1-\gamma} - f_L^{1-\gamma}) \left(1 + q \frac{r_j - r_0}{r_0} \right) \frac{r_j}{c} \\ &\quad - \pi \kappa_0 (f_H - f_L) \end{aligned} \quad (3)$$

Therefore, the system of N equations arises of the form

$$y_j = F_j(x_k) + \varepsilon_j \quad (4)$$

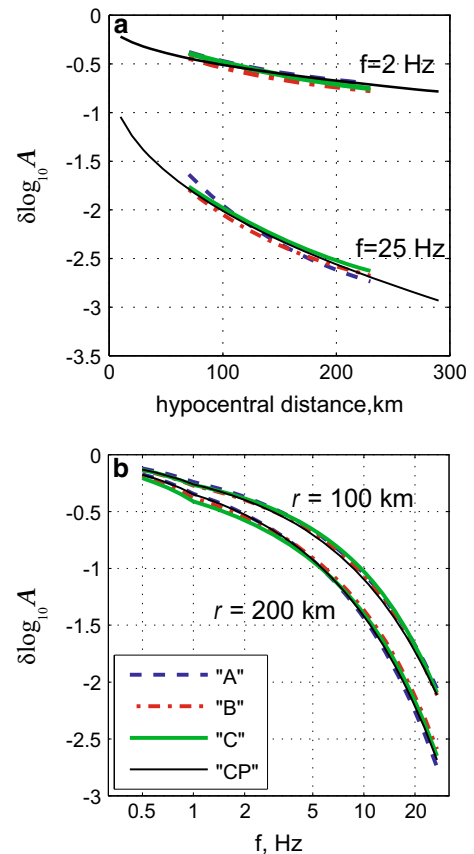


Figure 7

Comparison between trends of loss $\delta \log_{10} A(f) = \log_{10}(A(f)/A_0(f))$ (see Eq. 1) with respect to distance (left box) and frequency (right box) for the discussed attenuation models. For model denotations see Table 1

where ε_j is random error, assumed Gaussian with zero mean. The cases with $f_H - f_L < 2$ Hz were considered as unreliable, and were discarded. The employed non-linear inversion procedure was the Nelder–Mead simplex method that converged in a stable manner. The result—the “B” model—is given in Table 1, with error bounds, and $Q(f)$ is shown in Fig. 3. The error bounds were determined using the “delete-d jackknife method” (Wu 1990). The rms residual of fitting y_j values [i.e., $\sigma(\varepsilon_j)$] is about 0.07 (Fig. 6).

Determination of f_{ci} was repeated using the new “B” attenuation model and the augmented data set (563 spectra). It should be noted that for the records of the initial data subset (433 spectra), the replacement of the “A” attenuation model by the “B” one resulted, mostly, in insignificant changes of picks of f_{ci} or of f_L , f_H pairs. This stage of study is described in (GUSEV and GUSEVA 2016) in detail. To verify the stability of results, the third successive “C” attenuation model was obtained by inversion of the new set of y_j (determined now using the “B” model). The residuals of this inversion are shown in Fig. 6. In Fig. 3, one can compare $Q(f)$ for the initial and the two successively inverted models. This comparison does not make a full picture because the effect of large uncertainty and related variations of κ_0 estimates perturbs $Q(f)$ and makes impression of instable convergence. More indicative are spectral corrections $\delta \log_{10} A(f) = \log_{10} A(f)/A_0(f)$ predicted by each of the models (see Eq. 1); these are compared in Fig. 7. The difference of spectral corrections between initial and any of the inverted models in the distance range 80–220 km and over the full frequency band is limited. The difference between loss estimates predicted by the two inverted models “B” and “C” is minor, and one can believe that the practical convergence is attained, and that for the distance range studied, the average attenuation model for the vicinity of station PET is established rather reliably. Still, the value of κ_0 obtained by inversion seems somewhat too high for a hard-rock station like PET, probably because of the complete lack of data at short distances. In such a case, the estimate of κ_0 obtained in the inversion represents not only the site-dependent loss as such, but also the unknown and seemingly highly significant deviation (enhancement) of the loss at distances below

80–100 km as compared to the assumed linear distance dependence of Q^{-1} . This view is supported by examination of spectra of three rare small shocks occurred within the 30-km radius from PET, recorded by different instruments. Their spectra suggest that the true value of κ_0 for PET is close to 0.015. Nevertheless, Fig. 7 shows that the total loss correction is estimated in a stable manner.

Let us now discuss whether the obtained attenuation model can be confidently used for reduction of spectra. One should discriminate between a model that is sufficiently accurate to be usable for this aim, and another (imaginable but absent) model that contains accurate parameter estimates. It should be admitted that there is a significant correlation (tradeoff) between estimates of all four x_k . As a result, the obtained model can be reliably used only within the distance range studied. The mentioned tradeoff is complicated because, e.g., perturbing κ_0 affects both Q_0 and γ . Thus, no good estimate of site-related f_{max} in a strict sense is obtained; and the resulting κ_0 value should not be used for prediction of strong motion from earthquakes located near to PET. Such estimates are not much needed, however, because of low local seismicity of the Kamchatka land. The sources of threatening M8–M9 earthquakes are located at the same 80–150 km from the inhabited coast as those of small events under study; therefore, it is quite tolerable to use the obtained joint (κ_0 plus Q) loss estimates for engineering applications.

It was still expedient, mostly for eventual use in earthquake engineering applications, to develop a preliminary attenuation model for a somewhat wider distance range. This model had to extrapolate the distance trend of $\log_{10} A(f)$, found above, beyond the range 80–220 km where it was determined, and simultaneously to fulfill the following additional requirements: to fit the preliminary estimate of true κ_0 of PET, equal to 0.015 s; to exclude the physically inadequate linear distance dependence in (2) that predicts negative Q at a sufficiently large distance; and to explain a slight positive deviation of $\delta \log_{10} A(f)$ residuals as seen in Fig. 6b, that clearly indicates that the assumed linear trend is too gradual at small distances. By trial and error, the following preliminary model for $Q(f, r)$ was found, denoted

“CP”; it consists of the formula that replaces the linear trend of (2) by power law with exponent p :

$$Q^{-1}(f, r) = Q_0^{-1} \left(\frac{f}{f_0} \right)^{-\gamma} \left(\frac{r}{r_0} \right)^p \quad (5)$$

and the following set of parameters: $r_0 = 100$ km, $f_0 = 1$ Hz, $Q_0 = 150$; $p = -0.55$; $\gamma = 0.43$; all this to be combined with $\kappa_0 = 0.015$. The deviation of the γ value from one in the “B” and “C” model is noticeable; it hardly has geophysical meaning, however. It evidently results from the expressed correlation between κ_0 and γ : the lower the κ_0 , the smaller part of attenuation at HF it explains, pressing γ to get lower. For the distance range 80–220 km the modified model predicts $\log_{10}A(f)$ trend close to one determined above by inversion (see Fig. 7). Simultaneously it provides a more appropriate description outside this range. Equation 5 and the set of its parameters may provide a reasonable first approximation for attenuation over the Kamchatka subduction zone within the 40–300 km distance range.

5. Refined Estimates of Scaling of the Three Corner Frequencies

With more than 500 $\{f_{c1}, f_{c2}, f_{c3}\}$ triples at hand (some of them incomplete), it was possible to establish scaling behavior of each of these parameters and to inter-compare the f_{ci} vs. M_0 trends. The scaling behavior of f_{ci} for Kamchatka was first studied in (GUSEV and GUSEVA 2014) using the “A” attenuation model and the same data set as used above for retrieving the “B” attenuation model. Entire processing was repeated with the “B” attenuation model, resulting in new f_{ci} and spectral level picks (that were used to derive the “C” attenuation model discussed above). The adjustments were rather limited. In this repeated processing, however, the rejection of cases with insufficiently certain $d(f)$ and $a(f)$ plateaus was done more strictly, to improve the reliability of the resulting trends. The ultimate goal was to refine the estimates of scaling exponents β_i , $i = 1, 2, 3$ for the relationships of the kind $f_{ci} \propto M_0^{-\beta_i}$

To increase the amount of data, this scaling was determined in an indirect way, using local Kamchatka magnitude M_L as the main independent variable in the scaling study. The reason is that more than 15 % of analyzed spectra did not permit to estimate reliably the level of the LF plateau of $d(f)$, and that many earthquakes had no independent and reliable M_0 estimates. With this plan in mind, it was needed to verify in advance that M_L can supply an acceptable estimate of M_0 . To check this, the picked levels $d(f)_{f \rightarrow 0}$ were converted to M_0 and then to M_w , assuming $1/r$ geometric spreading, $c_S = 3.8$ km/s and average S -wave radiation pattern. The values of these local M_w estimates based on medium-period S -waves occurred to be well correlated with the teleseismic surface-wave estimates. The following average relationships were found: $M_L = M_w(\text{GCMT}) + 0.15$; $M_L = M_w(\text{PET } S\text{-waves}) + 0.35$, and therefore $M_w(\text{PET } S\text{-waves}) = M_w(\text{GCMT}) - 0.2$. The misfit of this kind was considered tolerable. The slope of the $M_L(M_w)$ trend deviates negligibly from the value 1.00 common for the magnitude range studied; thus in the scaling analysis, scaling exponents determined with respect to M_L were converted to β_i merely by multiplication by $2/3$. In a number of cases, published M_w vs. f_{ci} trends were compared to our f_{ci} vs. M_L results; in such cases, it was assumed that $M_w = M_L - 0.35$.

The results of scaling analysis are shown in Fig. 8. The scaling for f_{c1} and f_{c2} is seen in Fig. 8a, b. The accurate estimation of β_i may be hindered by the uncertainty in the exact balance of scatter of the points in Fig. 8a, b along abscissa and ordinate. When the abscissa values are not exact, the slope estimates obtained through ordinary regression shall have negative bias. To overcome this difficulty, orthogonal regression can be applied. Unfortunately, to obtain fully definite estimate in this way, one should fix the ratio ρ of variances along abscissa and ordinate, therefore, a new problem arises. To bracket the true value of f_{c1} , two variants of ρ were tried: $\rho = 0$ (ordinary regression), that resulted in $\beta_1 = \beta_{1rg} = 0.26 \pm 0.03$; and $\rho = 1$, giving $\beta_1 = \beta_{1or} = 0.33 \pm 0.03$ (preferred). The range of uncertainty is 0.07, wider than formal accuracy estimates. As β_{1or} closely reproduces the prediction of

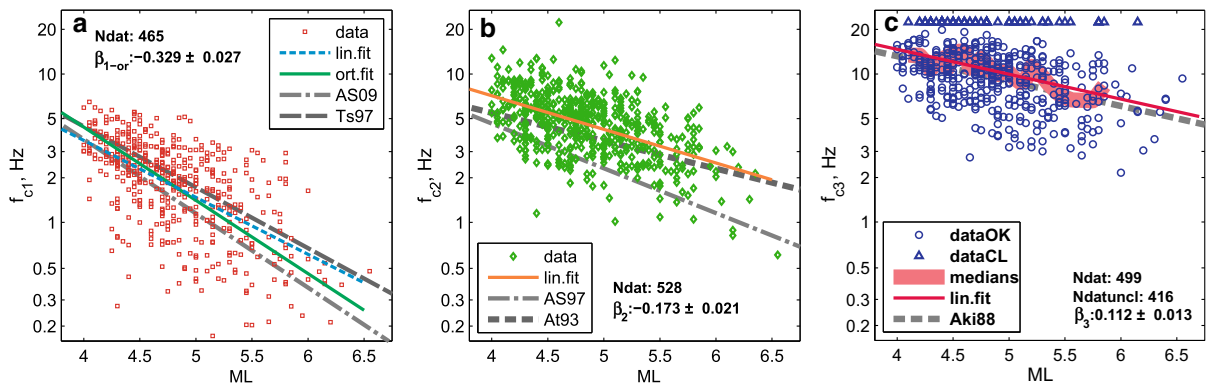


Figure 8

Empirical scaling of corner frequencies of Kamchatka earthquakes. For all plots: “lin.fit”—ordinary regression; “ort.fit”—orthogonal regression; the amount of usable data is shown as “Ndat”, and preferred β_i estimates are given. **a** Data on f_{c1} (squares); “AS09”—global trend after ALLMANN and SHEARER (2009), it follows similarity; “Ts97”—Taiwan trend after TSAI (1997). **b** Data on f_{c2} (diamonds), AS97—trend for Western United States after ATKINSON and SILVA (1997); At93—trend for Eastern North America after ATKINSON (1993). **c** “dataOK”—regular (M_L, f_{c3}) pairs; “dataCL”—clipped data (defined by the inequality $f_{c3} > 22$ Hz); “medians”—all data smoothed by running median; “lin.fit” approximates these medians; “Aki88”—the trend compiled by AKI (1988) from various sources; “Ndatuncl” is the amount of unclipped data. For readability, imported trends are shown beyond their original, data-supported range

the similarity hypothesis (of $\beta_1 = 1/3$) we can infer that data, rather, support this hypothesis, and in no way contradicts it.

For β_2 and β_3 we confined our analysis by ordinary regression. The slope of the log f_{c2} vs. M_L relationship, $\beta_2 = 0.17 \pm 0.02$, is evidently more gradual than that for log f_{c1} . The difference is statistically highly significant, and one can infer that the deviation of scaling behavior of f_{c2} with respect to that of f_{c1} , or, equivalently in our case, with respect to the value expected in the case of similarity, is real and well expressed.

Another interesting point is the difference between the values of f_{c1} and f_{c2} of the same event. The ratio f_{c2}/f_{c1} defines the width of the plateau of $v(f)$ spectrum, i.e., the degree of deviation of the event spectrum from the single-corner ω^{-2} model. Setting the threshold value for f_{c2}/f_{c1} equal to 2.0, we find that 62 % of data has higher f_{c2}/f_{c1} values, and thus are certainly of the double-corner kind. 38 % of spectra, in their LF part, either agree with the simple ω^{-2} model, or show only limited deviation from it.

In Fig. 8c, one can see the relationship $f_{c3}(M_L)$. Taking into account certain scatter of Q values among paths from different hypocenters, the estimates of f_{c3} exceeding 22 Hz were considered as insufficiently reliable. Such data were put into the category “ $f_{c3} > 22$ Hz,” and into the same category the cases were also included

when no third corner is seen at all but the spectrum is discernible at least up to 22 Hz. Cases when the $a(f)$ shape was apparently flat but dived under noise below 22 Hz were excluded from this analysis. The cases of the category “ $f_{c3} > 22$ Hz” are marked by triangles drawn at $f = 22$ Hz. About 20 % of f_{c3} estimates were of this “inequality” kind. Despite such “clipping”, the tendency of decay of f_{c3} with magnitude is evident. To reveal it reliably, medians of the f_{c3} data were calculated in moving window along the M_L axis. Median is not biased by clipping until it affects more than 50 % of data within a window, and clipping was rarely so strong. Linear regression applied to medians resulted in the estimate $\beta_3 = 0.11 \pm 0.013$. Therefore, the violation of similarity for f_{c3} is even sharper than for f_{c2} . It should be emphasized that each of the two established facts is of importance: one is that the scaling exponents, both for f_{c2} and f_{c3} , are significantly below that of f_{c1} , or, equivalently, below 1/3; another is that the scaling exponents for f_{c2} and f_{c3} differ significantly one with respect to another.

It was of certain interest to determine scaling exponents η_2 and η_3 in the relationships $f_{c2} \propto f_{c1}^{-\eta_2}$, $f_{c3} \propto f_{c1}^{-\eta_3}$. This can be done taking the ratios β_2/β_1 and β_3/β_1 that results in $\eta_2 = 0.52$ and $\eta_3 = 0.33$. Alternatively, by the direct juxtaposition of log f_{ci} and using the adequate procedure of orthogonal regression at $\rho = 1$, we find $\eta_2 = 0.51$, $\eta_3 = 0.35$ (preferred). The estimates of the two kinds

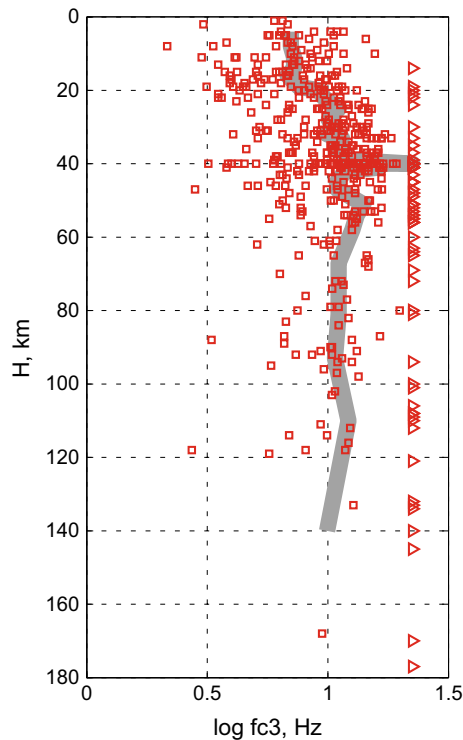


Figure 9

Third corner frequency f_{c3} estimates plotted against depth H . Dots and triangle marks are explained in the caption of Fig. 8c. Gray line shows running median. The anomaly at $H = 40$ km is related to the fact that local network produces a significant proportion of “40 km” depths that are highly unreliable. For unclear reason, these data had an excessive proportion of high- f_{c3} estimates

fit well, and the general picture ($\eta_2 < 1$, $\eta_3 < 1$, $\eta_3 < \eta_2$) can be considered as well established.

The depth dependence of f_{c3} (Fig. 9) was examined. For the depth range 0–50 km, the tendency of f_{c3} to increase with depth is well expressed. Deeper 50 km, this trend saturates. The fact of the depth dependence of f_{c3} is remarkable; it also provides an additional support to the idea of its existence. One can hardly expect such dependence if the estimates of f_{c3} are fictitious, and produced by data fluctuations and/or processing noise.

6. Discussion and Interpretation

6.1. On Attenuation

The approach developed here for determination of average attenuation has its limits. In our case when

small-distance data are lacking, one cannot determine κ_0 accurately, and an error in κ_0 translates into an error in absolute Q values, especially when Q is distance dependent. Still, the approach used is relatively well adapted for the limited aim of determination of spectral corrections that might recover source spectrum from an observed one, and this is just the kind of use on which the present study is concentrated. In addition, despite possible correlated errors in individual parameters, the recovered attenuation estimates can be employed for realistic prediction of scenario strong motions within the limited distance range studied; and this is just the range where such estimates are most needed for the case of Eastern Kamchatka. Still, the principal deficiency of the spectral method—its assumption of flat source acceleration spectra—cannot be overcome with the present approach.

Alternatively, one might directly use the distance decay of spectral amplitude to recover attenuation structure in an independent way. It should be understood, however, that the distance decay approach cannot produce κ_0 estimate; thus its results can provide only an incomplete description of attenuation. In addition, an a priori geometrical spreading model is needed for its applicability. Therefore, only the joint use of the two methods may permit to construct a fully reliable average attenuation model. This study is in progress, and the preliminary work (Gusev, Guseva, report at the 26th IUGG GA, Prague 2015) resulted in $Q(f)$ model (see Fig. 3) that well agrees with the “C” model described here.

After 3D attenuation tomography studies in subduction zones (e.g., STACHNIK and ABERS 2004; NAKAJIMA *et al.* 2013; LIU and ZHAO 2015) one might believe that the developed attenuation model is too simplistic. Tomographic studies show, however, that the subduction zone attenuation structure for a comparable forearc area, as recovered, e.g., by LIU and ZHAO (2015), shows only limited spatial variation. They systematically recover decrease of Q_S^{-1} with depth; and this feature seems to be incorporated into the distance decrease of Q_S^{-1} of our inversion. With this factor included into our list of unknowns, depth dependence of our residuals shows no significant anomaly. Numerical values of Q_S^{-1} are difficult

to compare because Liu and Zhao assume frequency-independent Q ; our early estimate of this kind equals 720, in reasonable agreement with their results that show the range of 550–880 for the comparable volume of Japan arc. NAKAJIMA *et al.* (2013), as well as other studies, also did not reveal any expressed variation of Q^{-1} (in addition to the mentioned vertical decrease) within and above the subducted slab; this is valid, however, only at a considerable distance from the volcanic chain.

6.2. On Scaling of f_{c2}

In Introduction, we mentioned the general problem of scaling and its relation to the similarity concept. Let us now discuss the observed scaling of f_{c2} and its possible meaning. The existence of f_{c2} was implicit in the study by AKI (1967) and noted by BRUNE (1970). The deviation of its trend from simple similarity ($\beta_2 < 1/3$) is no news as well (GUSEV 1983; IZUTANI 1984; ATKINSON 1993), and should be considered as a common tendency. See GUSEV (2013a) for a review of the observed f_{c2} trends, in overwhelming majority with $\beta_2 < 1/3$. The slope of the trend found here agrees well with the evidence collected in that review. However, the absolute level of Kamchatka f_{c2} data is relatively high, comparable to the estimates of ATKINSON (1993). This fact is correlated with similar deviation for f_{c1} that indicates relatively high-stress drop for our earthquake population, analogous to that for Taiwan data (TSAI 1997).

Let us introduce characteristic times, related to frequencies f_{c1} and f_{c2} , as $t_{c1} = 1/f_{c1}$ (related to rupture formation time T), and $t_{c2} = 1/f_{c2}$, correspondingly. It is common to relate t_{c1} to rupture formation time T . As for t_{c2} , modern textbooks, e.g., SHEARER (1999), relate it to rise time T_r of local slip; its possible stochastic version is the correlation time of local slip history at a point on the fault (AKI 1967). For the case of commonly assumed rupture propagation at an (average) velocity v_r , instant slip occupies at any time a certain strip [called “slip pulse” by HEATON (1990)] of a limited width $l = v_r T_r$. The strip sweeps entire fault of length L during time $T = L/v_r$. Let the relative strip width be $C_H = l/L = T_r/T$. GUSEV (2013b, 2014) noted that the ratio f_{c1}/f_{c2} must be comparable to C_H , and substantiated this view

using numerical simulation of a stochastic fault. The data collected here suggest that C_H systematically decreases with increasing magnitude: f_{c1}/f_{c2} varies from about 0.4 at $M_L = 4.5$ to about 0.15–0.12 at $M_L = 6$ –6.5. The latter number fits fairly well the typical value C_H , on the order of 0.1, proposed by HEATON (1990) on the basis of inverted space–time histories of earthquake sources of magnitude around 6–7. It should be noted, however, that in studies by AKI (1988), and PAPAGEORGIOU and AKI (1983), t_{c2} is understood in another way and related to the rupture duration of a subsource, and/or to the delay between sequential subsource initiation (i.e., between sequential crossing of barriers).

Let us consider now scaling of the characteristic times, taking t_{c1} (i.e., T) as the independent variable. From $f_{c2} \propto f_{c1}^{-\eta_2}$ we arrive to $t_{c2} \propto t_{c1}^{\eta_2}$, where the value of η_2 is close to 0.5. The simple fact that η_2 is definitely below unity may be understood as a qualitative indication of the tendency for slip pulse width to grow slower than in direct proportion to rupture size (as simple similarity would require). However, the fact that, approximately, $t_{c2} \propto t_{c1}^{1/2}$ may be understood as indicating that a propagating slip pulse broadens by some random mechanism that reminds random walk. In other words, the advancement of the ruptured area can be likened to random walk with drift, or diffusion with drift (FELLER 1957). Square root scaling is inherent for this class of processes. But this model, reasonable for 1D case, is doubtful for the random spreading of a ruptured area in 2D. No new theory is needed for this case. The assumedly random growth of a fault rupture area resembles many other random growth phenomena which were intensively studied during last decades, see the work by HALPIN-HEALY (1995).

Among the models of 2D growth, the simplest applicable one is that of Eden growth which describes, e.g., the growth of colonies of bacteria or clusters of molecules. These 2D aggregates grow by accumulation of material at their boundary. This accumulation is random, and the randomness results in non-smooth, convoluted, random “fractal” shape of the boundary. For the increase of rms width w of this “fringe-boundary” with increasing size l of the aggregate, power law holds: $w \propto l^\nu$. For different variants of the properties of the substrate

(homogeneous or “disordered”) the values of η between 0.33 and 0.68 are predicted. Our estimate of $\eta_2 \approx 0.5$ is well within these bounds. This makes the random growth hypothesis quite plausible. In should be noted, however, that in the above discussion of rupture growth model, an important implicit assumption is made: it is believed that the multitude of studied earthquake sources of various sizes can be considered as the set of snapshots of a growing earthquake source of gradually increasing length and magnitude.

6.3. On Scaling of f_{c3}

The important points regarding f_{c3} are: the mere existence of this feature, its nature, and its scaling. The existence of source-controlled f_{max} , or f_{c3} , was a matter of a long dispute. For instance, AKI (1988) noticed magnitude dependence of f_{max} for California earthquake data, and treated it as source effect; ATKINSON and SILVA (1997), however, relate this fact to amplitude dependence of κ_0 . Still, more and more evidence is accumulating that supports the existence of source contribution to f_{max} filter. See the study by GUSEV (2013a) for a review of relevant publications up to 2010. A few hypotheses have been proposed to explain formation of the third corner of source spectrum. Within the limits of the infinitesimally thin source-crack model, it was associated with cohesion zone width of a crack (CAMPILLO 1983; FUJIWARA and IRIKURA 1991; AKI 1988). Other, not necessarily opposing, view was expressed by PAPAGEORGIOU and AKI (1983) who associated f_{max} with the value of width of a “thick” fault zone. GUSEV (1990) considered f_{max} from a different viewpoint, in the context of fractal heterogeneity of a fault. This idea goes back to ANDREWS (1980) who considered a 2D random field of local stress drop with power-law spectrum; but Andrews did not discuss any high-wavenumber limit for this spectrum. GUSEV (1990) proposed that the source-controlled f_{max} is an imprint of the characteristic size that defines the lower limit for the size (wavelength) distribution of strength heterogeneity over the fault surface. Within the concept of band-limited fractal, this limit represents the lower fractal size limit of 2D fault heterogeneity,

whereas for longer size scales this heterogeneity can be assumed self-similar.

An analogous concept was proposed by YOKOI and IRIKURA (1991): they associated f_{max} with the smallest between-barrier interval on a fault that is covered by a hierarchy of such barriers with various characteristic interbarrier distances and various strengths. The next achievement in this line is the study, by DUNHAM *et al.* (2011), of a fault with fractally corrugated profile surrounded by plastic zone; the source-controlled f_{max} feature was, in essence, successfully simulated. This line of study should not be confused with the complementary but different AKI's (1988) suggestion to consider the same size as the upper fractal size limit of the “out-of-plane”, 3D fracture system located within the “thick” fault zone. All the listed possibilities for f_{c3} formation are far from being mutually exclusive; instead, they may well act cooperatively, or represent various facets of a complex picture. In a recent paper, WEN and CHEN (2012) analyzed variations of f_{max} (considered as source-controlled) along the causative fault of 2008 Wenchuan earthquake. They found that mainshock f_{max} , determined on near-fault accelerometers, correlates with the distance from the middle part of the fault, with typical values 5 Hz in its central part and 12 Hz at the periphery. They cite experimental estimates of the fault zone waveguide thickness that seem to indicate that this thickness decreases from the central part of the fault to its periphery in the manner well correlated with corresponding $1/f_{max}$ values; this may provide a direct experimental support to the “thick fault” concept of PAPAGEORGIOU and AKI (1983). Wen and Chen themselves associate v_r/f_{max} with the cohesion zone width of a crack subfault.

Let us now discuss the possible meaning of the trend of f_{c3} vs. M_0 and physics that underlies it. The decrease of f_{c3} with M_0 is found here to be slow: $f_{c3} \propto M_0^{-0.11}$. A trend of this kind was first found by AKI (1988), whose estimate $\beta_3 = 0.105$ is essentially reproduced in our data. A comparable trend was found earlier by FACCIOLI (1986), however, he was inclined to treat f_{max} as mostly attenuation effect. Less clear indications of a similar trend, in terms of κ_{event} vs. M dependence, were noted by Purvance and ANDERSON

(2003). It should be noted that ATKINSON and SILVA (1997), however, confirming the fact of magnitude dependence of f_{\max} (in the form κ_0), ascribe its origin to non-linear amplitude dependence of κ_0 . In our case, magnitude dependence is well expressed. As KILB *et al.* (2012) note, the threshold for significant non-linearity is on the order of tens of gals, much above the amplitude range of our records. This means that in our case, the magnitude dependence can be safely considered as evidence supporting the existence of f_{c3} . The depth dependence gives another similar argument. Assuming f_{c3} as existent, and its magnitude dependence as real for our data, we can infer that lower fractal limit of fault heterogeneity increases with source size, however, slowly.

A tectonophysical cause of such a tendency may lay in variations of fault surface maturity: the greater is the distance slipped (in geological time scale) by a fault wall along its counterpart, the larger is associated wear/damage (GUSEV 1990; MATSU'URA *et al.* 1992; PURVANCE and ANDERSON 2003). In this process, shorter wavelengths of the fault profile are ground away faster and the upper cutoff of heterogeneity spectrum shifts down, to lower wavenumbers and longer wavelengths. In parallel, the damaged fault zone grows thicker. Wear operates twofold: by selective abrasion of smaller asperities of fault relief, and by accumulation of debris that plaster up other smaller asperities; each of these tendencies shifts f_{c3} down. The property of maturity can well be related to magnitude. One can expect a positive relationship: the larger is the magnitude of an earthquake, the larger are chances that its fault walls traveled farther along each other, and the larger effects of wear one can expect. There are, however, processes that counteract wear: "healing" or strength recovery of a fault (by reestablishment of monolithic state through such processes as recrystallization of crushed gauge and/or geothermally induced sedimentation) and wandering of individual fault paths of successive events within a much broader fault zone, which can be seen on the day surface as a bundle of fault branches. We believe, however, that these tendencies can only partly suppress the effects of wear processes discussed earlier.

The depth trend of Fig. 9 agrees with this explanation. One can expect that the healing processes are amplified at larger depths, resulting in a relative decrease of the upper cutoff of the fault

heterogeneity size distribution, and in a corresponding increase of f_{c3} . The trend of Fig. 9 agrees well with the results of IWAKIRI and HOSHIBA (2012) who analyzed time-dependent f_{\max} which was observed on the accelerograms of the developing rupture of the 2011 Tohoku mega-earthquake. They found that f_{\max} increased during the propagation of the rupture front to larger depths. They found some additional support to the depth dependence of f_{\max} analyzing acceleration spectral ratios of three pairs of large earthquakes whose sources were located at different depths.

7. Conclusion

An attempt of separation of source-controlled and attenuation-controlled constituents of f_{\max} is undertaken using data on 563 moderate-sized earthquakes of Kamchatka subduction zone recorded by PET station. To perform this more accurately, first an initial attenuation model for the lithosphere around PET was compiled. Then, using the spectral approach, a more reliable model was obtained by iterations of non-linear inversion. In each inversion, for each spectrum, the usable segment of frequency axis was selected where one could believe the source acceleration spectrum to be flat. After two repetitions the difference between attenuation models obtained in the two inversions was found to be minor; therefore the stability of the employed approach was verified. The resulting attenuation model could be employed for confident recovery of majority of source spectra up to 22 Hz.

Among 499 attenuation-corrected spectra of $M = 4-6.5$ local earthquakes with sufficient S/N ratio at HF, a large fraction (>80 %) manifests the source-controlled f_{\max} , i.e., the third corner frequency f_{c3} . The values of f_{c3} lie in the range 3–20 Hz; on the average, they slowly decay with magnitude. These values also show considerable dependence on hypocentral depth over the upper 0–50 km layer: the deeper an event is located, the higher is f_{c3} . The magnitude dependence of f_{c3} agrees well with pioneering works of FACCIOLO (1986) and AKI (1988). In their lower frequency part, about 2/3 of spectra shows clear second corner; for the rest 1/3, the standard one-corner ω^{-2} spectral model can be considered as a good approximation.

Clear deviations from similarity were found for scaling of f_{c2} and f_{c3} . These deviations permit to make some deductions regarding physical processes in the earthquake source. The tendency $f_{c2} \propto f_{c1}^{0.5}$ may indicate that during the spreading of the ruptured area over a geological fault, the growth of this area may obey a stochastic model of random surface growth, like Eden model or its generalizations. The tendency $f_{c3} \propto M_0^{-0.11}$ may reflect the magnitude dependence of the characteristic size of fault surface heterogeneity.

Acknowledgments

The study was supported by the grant from the Russian Science Foundation (project #14-17-00621), and was performed at the Kamchatka Branch of the Geophysical Service of Russian Ac. Sci. Valuable comments of A. Baltay and of two anonymous reviewers are appreciated.

REFERENCES

- ABUBAKIROV, I. R. (2005), *Attenuation characteristics of transverse waves in the lithosphere of Kamchatka estimated from observations at the Petropavlovsk digital broadband station*, *Izvestiya, Physics of the Solid Earth*, 41: 813–824. (original in Russian: *Fizika Zemli*, 2005, #10, 46–58).
- ABUBAKIROV I.R. and GUSEV. A.A. (1990), *Estimation of scattering properties of lithosphere of Kamchatka based on Monte-Carlo simulation of record envelope of a near earthquake*. *Phys. Earth Planet. Inter.* 64, 52–67.
- AKI, K. (1967), *Scaling law of seismic spectrum*. *J. Geophys. Res.* 72, 1217–1231.
- AKI, K., (1988), *Physical theory of earthquakes*, in *Seismic Hazard in Mediterranean Region*, 3–34. ed. J. Bonin, M. Cara, M. Cisternas, R. Fantechi, Kluwer Academic Publ.,
- ALLMANN, B. P., and P. M. SHEARER (2009), *Global variations of stress drop for moderate to large earthquakes*, *J. Geophys. Res.*, 114, B01310, doi:10.1029/2008JB005821.
- ANDERSON, J. G. and HOUGH, S. E. (1984), *A model for the shape of the Fourier amplitude spectrum of acceleration at high frequencies*. *Bull. Seism. Soc. Am.*, 74, 1969–1993.
- ANDERSON, J. G. (1991), *A preliminary descriptive model for the distance dependence of the spectral decay parameter in Southern California*. *Bull. Seism. Soc. Am.*, 81, 2186–2193.
- ANDREWS D.J. (1980), *A stochastic fault model, 1: Static Case*, *J. Geophys. Res.*, 78, 3867–3877.
- ATKINSON, G. (1993), *Source spectra for earthquakes in eastern North America*, *Bull. Seism. Soc. Am.* 83, 1778–1798.
- ATKINSON, G. (1996) *The High-Frequency Shape of the Source Spectrum for Earthquakes in Eastern and Western Canada*, *Bull. Seism. Soc. Am.* 86, 106–112.
- ATKINSON, G., and W. SILVA (1997), *Empirical source spectra for California earthquakes*, *Bull. Seism. Soc. Am.* 87, 97–113.
- BALTAY, A., S. IDE, G. PRIETO, and G. BEROZA (2011) *Variability in earthquake stress drop and apparent stress*. *Geophys. Res. Lett.* 38, L06303, doi:10.1029/2011GL046698.
- BOATWRIGHT, J. (1978), *Detailed spectral analysis of two small New-York State earthquakes*. *Bull. Seismol. Soc. Am.*, 68, 1117–1131.
- BOORE, D.M. and W B. JOYNER (1997) *Site Amplifications for Generic Rock Sites*. *Bull. Seismol. Soc. Am.*, 87, 327–341.
- BRUNE, J. N. (1970), *Tectonic stress and spectra of seismic shear waves from earthquakes*. *J. Geophys. Res.*, 75, 4997–5009.
- CAMPILLO, M. (1983), *Numerical evaluation of the near-field high-frequency radiation from quasi-dynamic circular faults*, *Bull. Seism. Soc. Am.* 73, 723–734.
- DUNHAM, E.M., BELANGER, D., CONG, L., and KOZDON, J.E. (2011), *Earthquake ruptures with strongly rate-weakening friction and off-fault plasticity. Part 2: Nonplanar Faults*. *Bull. Seism. Soc. Am.*, 101, 2308–2322, doi: 10.1785/0120100076.
- EDWARDS, B. O.-J. KTEPIDOU, F. COTTON, N. ABRAHAMSON, Ch. VAN HOUTTE and D. FAH (2015). *Epistemic uncertainty and limitations of the κ_0 model for near-surface attenuation at hard rock sites*. *Geophys. J. Int.* (2015) 202, 1627–1645 doi: 10.1093/gji/ggv222.
- FACCIOLI, E. (1986), *A study of strong ground motions from Italy and Yugoslavia in terms of gross source properties*. *Geophys. Monog.*, 37, 297–309.
- Feller, W. *An Introduction to Probability Theory and Its Applications, Vol. 1, Ch. XIV*, (J. Wiley & Sons, New York, 1957).
- FUJIWARA, H. and IRIKURA, K. (1991), *High-frequency seismic wave radiation from antiplane cohesive zone model and f_{max} as source effect*. *Bull. Seism. Soc. Am.* 81, 1115–1128.
- GUSEV, A. A. (1983), *Descriptive statistical model of earthquake source radiation and its application to an estimation of short period strong motion*, *Geophys. J. R. Astr. Soc.* 74, 787–808.
- GUSEV A.A. (1990). *On relations between asperity population and earthquake population on a fault*. In *Extended Abstracts, International symposium on earthquake source physics and earthquake precursors*. (University of Tokyo, Tokyo). 140–142.
- GUSEV, A.A. (2013a) *High-frequency radiation from an earthquake fault: a review and a hypothesis of fractal rupture front geometry*. *Pure Appl. Geophys.* 170, 65–93. doi:10.1007/s00024-012-0455-y.
- GUSEV, A.A. (2013b) *Fractal earthquake source with slip zone generates acceleration time histories with flat spectra*. *Doklady Earth Sciences*, 448, 211–213. (original in Russian: *DAN*, 2013, 448, 465–467).
- GUSEV, A.A. (2014) *Doubly stochastic earthquake source model: “omega-square” spectrum and low high-frequency directivity revealed by numerical experiments*. *Pure Appl. Geophys.* 171, 2581–2599, doi 10.1007/s00024-013-0764-9.
- GUSEV, A. A., and SHUMILINA L. S. (2000) *MODELING THE INTENSITY MAGNITUDE-DISTANCE RELATION BASED ON THE CONCEPT OF AN INCOHERENT EXTENDED EARTHQUAKE SOURCE*, *Vulc. Seis.*, 21, 443–463 (English edition; original in Russian: 1999, #4–5, 29–40).
- GUSEV A.A. and GUSEVA E.M. (2012) *Testing the applicability of attenuation parameter “kappa” for fast rough estimation of hypocentral distance (using the data of station “Petropavlovsk”)*. In: *Seismological and geophysical observations on Kamchatka. Ch. 15*, 397–411. (eds Gordeev E.I. and Chebrov V.N.) (Novaya kniga, Petropavlovsk-Kamchatskii) (in Russian).

- GUSEV A.A., and GUSEVA E.M. (2016) Shear wave attenuation estimated from spectral decay rate in the vicinity of the Petropavlovsk Station, Kamchatka. *Izvestiya, Phys. Solid Earth* (in press).
- GUSEV A.A. and GUSEVA E.M. (2014), *Scaling properties of corner frequencies of Kamchatka earthquakes*. *Doklady Earth Sciences*, 2014, 458, 1112–1115. (English edition; original in Russian: *DAN*, 2014, 458, 88–91).
- HANKS, T. C. (1982), f_{max} . *Bull. Seismol. Soc Am*, 72, 1867–1879.
- HALPIN-HEALY, T., ZHANG Y.-Ch. (1995), *Kinetic roughening phenomena, stochastic growth, directed polymers and all that*. *Physics Reports*, 254, 215–414.
- HEATON, T. H., (1990), *Evidence for and implications of self healing pulses of slip in earthquake rupture*, *Phys. Earth Planet. Inter.*, 64, 1–20.
- IWAKIRI, K., and HOSHIBA, M. (2012), *High-frequency (> 10 Hz) content of the initial fifty seconds of waveforms from the 2011 Off the Pacific Coast of Tohoku earthquake*. *Bull. Seism. Soc. Am.* 102, 2232–2238, doi: [10.1785/0120110241](https://doi.org/10.1785/0120110241).
- IZUTANI, Y. (1984), *Source parameters relevant to heterogeneity of a fault plane*. *J. Phys. Earth*, 32, 511–529.
- JO, N., and BAAG, Ch.-E. (2007) *Estimation of site-dependent spectral decay parameter from earthquake ground motions in southern Korea*. *Geosciences J.*, 11, 165–174.
- JOYNER, W. B., (1984), A scaling law for the spectra of large earthquakes, *Bull. Seism. Soc. Am.*, 74, 1167–1188.
- KANAMORI, H., and ANDERSON, D. L. (1975), *Theoretical basis of some empirical relations in seismology*, *Bull. Seism. Soc. Am.*, 65, 1073–1095.
- KILB, D., G. BIASI, J. ANDERSON, J. BRUNE, ZH. PENG, and F. L. VERNON (2012) *A Comparison of Spectral Parameter Kappa from Small and Moderate Earthquakes Using Southern California ANZA Seismic Network Data*. *Bull Seism Soc Am*, 102, 284–300.
- KINOSHITA, S. (1992), *Local characteristics of the f_{max} of bedrock motion in the Tokyo metropolitan area, Japan*, *J. Phys. Earth*. 40, 487–515.
- LIU, X., and ZHAO, D., (2015), *Seismic attenuation tomography of the Southwest Japan arc: new insight into subduction dynamics*, *Geophys. J. Int.* 201, 135–156, doi:[10.1093/gji/ggv007](https://doi.org/10.1093/gji/ggv007).
- MATSU'URA, M., H. KATAOKA and B. SHIBAZAKI (1992), *Slip-dependent friction law and nucleation processes in earthquake rupture*, *Tectonophysics*, 211, 135–148.
- NAKAJIMA, J., SH. HADA, E. HAYAMI, N. UCHIDA, A. HASEGAWA, SH. YOSHIOKA, T. MATSUZAWA, and N. UMINO (2013), *Seismic attenuation beneath northeastern Japan: constraints on mantle dynamics and arc magmatism*. *J. Geophys. Res.*, 118, 1–18, doi:[10.1002/2013JB010388](https://doi.org/10.1002/2013JB010388).
- PAPAGEORGIOU, A. S. and K. AKI. (1983), *A specific barrier model for the quantitative description of the inhomogeneous faulting and the prediction of strong ground motion: I. Description of the model*. *Bull. Seism. Soc. Am.*, 73, pp. 693–722.
- POPESCU, E., M. POPA and M. RADULIAN (2003) *Efficiency of the spectral ratio method to constrain the source scaling properties of the Vrancea (Romania) subcrustal earthquakes*. *Romanian Repts. Phys.*, 55, 149–169.
- PURVANCE M. D. and ANDERSON, J. G. (2003). *A comprehensive study of the observed spectral decay in strong-motion accelerations recorded in Guerrero, Mexico*. *Bull. Seismol. Soc. Amer.*, 2003; 93; 2; 600–611; doi:[10.1785/0120020065](https://doi.org/10.1785/0120020065).
- SASATANI, T., (1997). *Source characteristics of the 1994 Hokkaido Toho-oki earthquake deduced from wide band strong-motion records*. *J. Fac. Sci. Hokkaido Univ. Ser. VII (Geophys.)* 10, 269–293.
- SATOH, T., KAWASE, H., and SATO, T. (1997), *Statistical spectral model of earthquakes in the Eastern Tohoku District, Japan, based on the surface and borehole records observed in Sendai*. *Bull. Seism. Soc. Am.*, 87, 446–462.
- SHEARER, P.M. (1999) *Introduction to Seismology*, Cambridge University Press, Cambridge.
- STACHNIK, J. C., G. A. ABERS, and D. H. CHRISTENSEN (2004), *Seismic attenuation and mantle wedge temperatures in the Alaska subduction zone*, *J. Geophys. Res.*, 109, B10304, doi:[10.1029/2004JB003018](https://doi.org/10.1029/2004JB003018).
- TSAI, Ch-Ch.P. (1997), *Relationships of seismic source scaling in the Taiwan region*, *TAO*, 8, 49–68.
- WEN, J., and CHEN, X.-F. (2012), *Variations in f_{max} along the ruptured fault during the Mw 7.9 Wenchuan Earthquake of 12 May 2008*. *Bull. Seism. Soc. Am.*, 102, 991–998, doi: [10.1785/0120110105](https://doi.org/10.1785/0120110105).
- WU, C. F. J. (1990), *On the asymptotic properties of the jackknife histogram*. *Annals of Statistics*, 18, 1438–1452.
- YOKOI, T., and IKIRURA, K. (1991), *Meaning of source-controlled F_{max} in the empirical Green's function technique based on ω^{-2} scaling law*. *Annals, Disast. Prev. Res. Inst. Kyoto Univ.*, No B-1, 177–189.